Journal of Electroceramics 4:1, 151–165, 2000


# Materials for Photonic Applications From Sol-Gel*

GIOVANNA BRUSATIN, MASSIMO GUGLIELMI, PLINIO INNOCENZI, ALESSANDRO MARTUCCI & GIOVANNI SCARINCI

*Dipartimento di Ingegneria Meccanica, Settore materiali, Università di Padova, via Marzolo 9, 35131 Padova, Italy*

Submitted March 10, 1999; Revised June 2, 1999; Accepted August 3, 1999

**Abstract.** A review of sol-gel materials developed in our laboratory for photonic applications is presented. These materials include planar and strip waveguides for integrated optics (IO) passive devices, Er doped waveguides for IO amplifiers, films doped with semiconductor quantum dots for optical switching and fullerene doped materials for optical limiting.

**Keywords:** sol-gel, integrated optics, waveguides, quantum dots, fullerene

## 1. Introduction

For fabricating integrated optic (IO) devices, sol-gel processing is an interesting alternative to other technologies such as flame hydrolysis deposition (FHD) and chemical vapour deposition (CVD), because of potential low costs and relative ease of production. Many kinds of materials for IO technologies have been prepared in many academic and industrial laboratories, even though commercial applications have not yet reached the market [1]. In our laboratory we have studied and developed several different materials for IO and photonic applications.

(1) Low loss planar waveguides of various compositions, as passive IO components, both inorganic and hybrid organic-inorganic, have been obtained, and strip waveguides have been fabricated by using laser densification. (2) Sol-gel planar waveguides have been doped with Er to obtain optically active components for amplifiers. (3) Waveguides doped with quantum dots for application in optical swithching have also been developed. Semiconductor nanoparticles have been used to dope the waveguides. (4) Hybrid organic-inorganic materials, as bulk and coating films, have been synthesised *ad hoc*, as host materials for optically active organic molecules. Fullerene derivatives have been successfully entrapped in hybrid matrices and optical limiting has been achieved.

*Article partially published in the *Proceedings of the Korea–Italy Joint Symposium on Electronic Ceramics*, Sept. 24, 1998, Kyungpook National University, Taegu, South Korea, Ed. By the Office of the Scientific Attaché of the Italian Embassy in Seoul.

## 2. Sol-gel Planar and Strip Waveguides

Several types of oxide and hybrid organic-inorganic waveguides were synthesised as passive components for integrated optics devices or hosts for optically active molecules. Low loss planar and strip waveguides of several oxide compositions were obtained [2–4]. The relationship between the optical losses and the surface and microstructure of the waveguides was studied [4–6].

### *2.1. Waveguide Preparation*

Sol-gel waveguides were prepared by acid catalysed solutions of alkoxides. To increase the refractive index of the material, titanium, zirconium, germanium or aluminium were co-hydrolised with silicon alkoxides; the control of the reaction rate was usually achieved by chelating agents. Dipping and spinning were used to deposit coating film layers on silicon and silica substrates. Inorganic oxide waveguides were obtained after firing at temperatures in the

range 500–700°C. The firing temperature was carefully chosen, as a function of the composition, to avoid crystallisation in the film. By this route the thickness of a single layer is usually in the range 0.1–0.5 $\mu$m and a multideposition process has to be employed to obtain thicker coatings suitable for IO devices. By co-hydrolysis of organically modified alkoxides, such as methyltriethoxysilane (MTES), with titanium or zirconium alkoxides, waveguides up to 1.8 $\mu$m thick per single layer were obtained. The films were fired at 500°C and did not crack because of the presence of the methyl groups that reduce the stress during drying. Hybrid organic-inorganic waveguides were also fabricated: 3-glycidoxy-propyltrimethoxysilane (GPTMS)-$TiO_2$ (70–30% molar ratio) and 3-(trimethoxysilil)-propyl methacrylate (TSPM)-$TiO_2$ (70–30%). Polymerization of the organic chains was achieved by titanium alkoxides with GPTMS and thermally with TSPM. 10–15 $\mu$m thick uncracked layers were obtained after 150°C baking treatments.

### 2.2. *Optical Losses*

To minimize waveguide losses is a very crucial point in IO applications. The fabrication of efficient Erbium doped waveguides for amplifiers, for instance, requires optical losses at least lower than 1 dB/cm [7]. The higher limit of the optical losses for passive components is usually fixed around 0.3 dB/cm. Waveguide losses, which are due to absorption and scattering of guided light, can be reduced through careful control of the microstructure of the waveguide material. The main causes of optical losses are volume induced scattering and the surface roughness scattering.

Other microstructural aspects can also play a very important role, such as residual porosity in the sol-gel guiding layer, the presence of residual carbon and non-bridging oxygens. The optical losses measured by m-line spectroscopy at $\lambda = 633$ nm were 0.3–0.2 dB/cm in $SiO_2$-$TiO_2$ inorganic samples and 0.4 dB/cm in hybrid waveguides.

### 2.3. *Strip Waveguides*

Strip waveguides were obtained by laser densification followed by chemical etching of the non-densified part of the film, as it is illustrated in Fig. 1. Following this method $SiO_2$-$TiO_2$ strip waveguides were obtained with optical losses larger than in the corresponding planar waveguides. The main source of optical losses, in laser densified waveguides from sol-gel, is the presence of residual carbon, because of the rapid densification induced by the patterning laser [3].

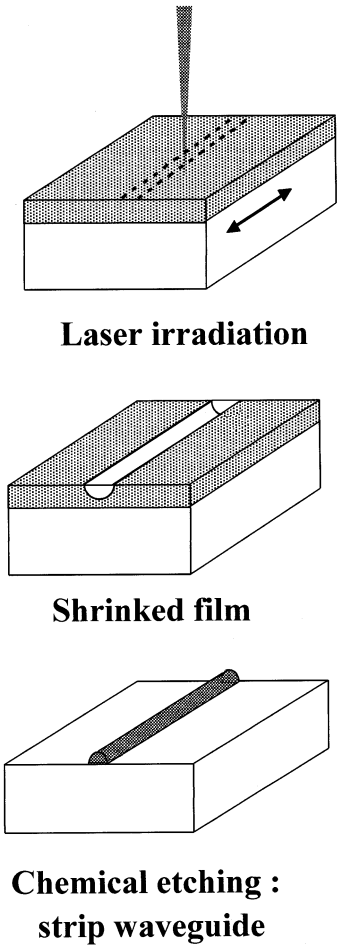


*Fig. 1.* Preparation process of laser densified strip waveguides.

## 3. Semiconductor Doped Sol-Gel Films for Switching and Non-Linear Devices

Thin films doped with semiconductor nanoparticles to obtain nonlinear planar waveguides were extensively studied by our group [8].

### *3.1. Preparation and Characterization of Semiconductor-Doped Planar Waveguides*

We initially used the synthetic route developed by Tohge and coworkers [9], because it offered a simple method for the preparation of a sol suitable for the deposition of thin films. A $30TiO_2$-$70SiO_2$ composition was used for the matrix because of its high refractive index. Tetraethoxysilane (TEOS) or methyltriethoxysilane (MTES) were pre-hydrolyzed under acidic conditions in an ethanol solution. A methanol solution of cadmium or lead acetate and thiourea was stabilized with acetylacetone (acacH) and mixed with the silica alkoxide sol. Titanium butoxide chelated with acacH was then added and the final sol was used to deposit thin films on glass slides by dip-coating. The waveguides obtained by heating the films at 500°C had a refractive index of about 1.68 and propagation losses, measured at 632.8 nm for CdS-doped samples and at 810 nm for PbS doped ones, below 1 dB/cm. Smaller indices and larger losses (anyway below 2 dB/cm) were found in films treated at 300°C.

XRD analysis performed on bulk samples and on films showed that the heat-treatment at 300°C was sufficient to decompose the complexes formed by reaction of metal salts with thiourea. The average crystal size, evaluated from broadening of diffraction lines by the Scherrer equation is reported in Table 1. The size of particles in thin films could be evaluated only for PbS-doped samples. They were much smaller then in bulk samples, probably because the particles have more time to aggregate in the sol before gelation takes place than in the liquid film where fast gelation occurs due to fast solvent evaporation. The growth of particles with heat treatment temperature is evident from the data of Table 1.

A TEM study done on doped silica and silica-titania samples produced by this method [10] showed that the matrix affects both the size and size distribution of sulfide particles. The comparison of spectrophotometric curves, XRD patterns and TEM images of silica and silica-titania films containing CdS or PbS showed that the particles were smaller and more narrowly distributed in the case of the silica-titania matrix. This difference was present in samples fired at different temperatures, even if an increase in size and a broadening in the size distribution was observed at higher temperatures. The difference may be the effect of a different growth of particles due to different microstructures in the two matrices, for example porosity and skeleton connectivity.

Non-linear measurements were done on CdS-doped films by a method based on the non-linear m-line technique. The film was deposited on a fused silica wafer where diffraction gratings had been previously ion-milled. For the measurement, the reflected/transmitted intensity of a well-collimated laser beam was recorded as a function of the incident angle. At high intensities the m-line associated with the excitation of the guided wave is shifted and its shape is changed with respect to the linear case. This leads to a measurement of the non-linear refractive index $n_2$ through a calculation of the efficiency of the non-linear distributed coupler. An OPO(Optical Parametric Oscillator)-laser pumped by the third harmonic of a seeded Nd:YAG laser was used as light source. The pulse duration was 8 ns and the repetition rate 10 Hz.

At the resonant wavelength of 450 nm a $n_2$ value of $-2.910^{-7}\,cm^2/kW$, corresponding to a $\chi^{(3)}$ of about $1.6\ 10^{-8}$ esu, was measured. Between 530 and 560 nm the value was one order of magnitude smaller. An example of measurement is presented in Fig. 2. The reversibility of the nonlinear effect was demonstrated by recording several successive cycles of low and high intensity curves.

These results were encouraging but not very reproducible. As previously discussed, the difference in size of nanoparticles in bulk samples and in films suggested that the colloidal sol was not stable and that particle growth changed the properties of the sol over time. Thus it was decided to use a different approach, by separating as much as possible the preparation of

*Table 1.* Average crystal size (nm) of semiconductor particles obtained in gel powders and films using thiourea as sulfidizing agent

| Powders | | | | Thin film | |
|---|---|---|---|---|---|
| CdS | | PbS | | PbS | |
| 300°C | 500°C | 300°C | 500°C | 300°C | 500°C |
| 3.5 | 5 | 25 | 31 | 3 | 4 |

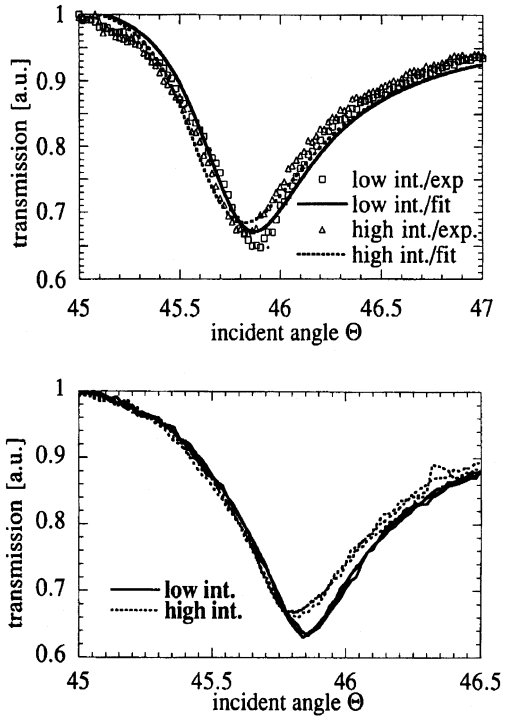


*Fig. 2.* Non-linear m-line measurement at 560 nm for a CdS-doped sample. Both experimental results and theoretical fitted curves are traced (top). The reversibility of the non-linear effect is checked by recording several cycles of low-high intensity curves (bottom).

nanoparticles and matrix by using the surface-capping method for the control of particle size. Films doped with CdS, PbS, HgS, $Pb_xCd_{1-x}S$ and $Hg_xCd_{1-x}S$ were prepared by this route.

Thioacetamide, TA, ($CH_3CSNH_2$) was used as a source of sulfur, as it readily reacts at room temperature to give sulfides [11], and 3-mercaptopropyltrimethoxysilane (3-MPTMS) was selected as a bifunctional surface-capping agent (SCA). Silica and silica-titania gels were used as matrices (the preparation of alkoxide solutions was the same as described above). The colloidal sulfide sols were added to the alkoxide solutions and the final sols were used for the deposition of thin films. These were deposited by the dip-coating method on soda-lime glass slides, dried at 60°C and fired at different temperatures. The details of the preparation procedure are reported in [12].

The XRD spectra of CdS and HgS powders obtained using different 3-MPTMS and TA amounts are shown in Fig. 3. CdS obtained without the surface capping agent $(M = 0)$ crystallized in the cubic zinc blende structure and the average crystal size was calculated to be about 3 nm. Instead, the particles obtained using 3-MPTMS exhibited very broad peaks mainly attributable to the hexagonal wurtzite type structure. The particle size in the sample with a ratio M of 3-MPTMS to metal of 0.5 was evaluated to be about 2 nm.

In the case of HgS the peaks were assigned to the cubic system, even though weak reflections of the hexagonal phase could not be excluded. Also in this case the effect of 3-MPTMS on particle size is evident: an average size of about 5 nm was calculated for the sample with $M = 0$ and much smaller sizes (presumably below 2 nm) were obtained by using the SCA. The absorption spectra of two colloidal sols

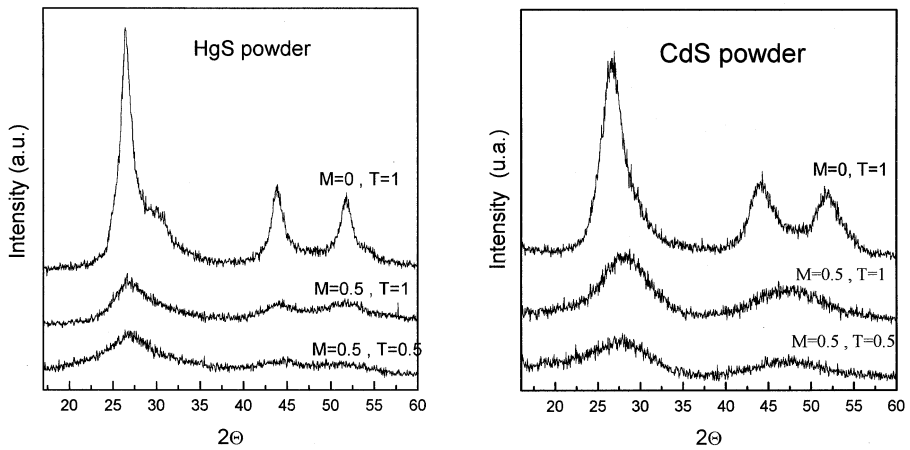


*Fig. 3.* XRD spectra of CdS and HgS powders obtained by precipitation from colloidal sols containing different amounts of 3-MPTMS ($M$ = 3-MPTMS/Cd) and TA ($T$ = Thioacetamide/Cd).

prepared with different MPTMS/TA ($M$) ratios are shown in Fig. 3. The absorption onsets are located at a wavelength much shorter than for bulk HgS, due to the quantum confinement effect. Furthermore, the blue-shift increases with $M$, confirming that smaller particles were obtained by increasing the $M$ ratio.

The thin silica or silica-titania films obtained from the doped precursor solutions and dried at 60°C exhibited almost the same blue-shift observed in the parent colloidal sol, indicating that the particle size did not change significantly during the mixing of solutions and deposition steps. The absorption curves of $SiO_2$ and $SiO_2$-$TiO_2$ thin films doped with colloidal sols obtained with $M = 0.5$ are reported in Fig. 4.

An interesting possibility to shift the absorption onset of semiconductor quantum dots is given by the change of nanoparticles composition in binary systems. This possibility was investigated by preparing $Hg_xCd_{1-x}S$ and $Pb_xCd_{1-x}S$ colloidal sols and doped films [13]. The UV-vis spectra of $Hg_xCd_{1-x}S$-doped silica films are reported in Fig. 5. The excitonic transition, taken at the minimum of the second derivative of the absorption spectrum, are located at 540, 520 and 410 nm in the samples doped with HgS, $Hg_{0.7}Cd_{0.3}S$ and $Hg_{0.3}Cd_{0.7}S$, respectively.

PbS doped materials were also synthesized because of their very interesting properties. The bulk absorption edge of PbS is around 3 $\mu$m, which can be shifted to 900 nm due to quantum confinement and large absorptions. Dispersive non-linearities are predicted for this material if the quantum dot transitions are not excessively broadened [14].

The procedure described previously for PbS was used to synthesize the other quantum dot doped materials. The XRD patterns confirmed that cubic (rock salt) PbS crystals were obtained at room temperature. The average crystal size ranged from 8 to 3.5 nm as the $M$ = MPTMS:Pb ratio changed from 0.5 to 2. Smaller crystals were found in the doped films obtained by mixing the alkoxide solution and the colloidal PbS sol. In silica-titania films obtained using a sol with $M = 0.5$ the average size was estimated to be about 4 nm. The absorption spectrum of a PbS-doped silica-titania film is shown in Fig. 6. The absorption edge exhibits a large shift with respect to bulk PbS and the long tail may be due to defect states, particle size distribution and/or indirect transition [15,16].

The direct band gap was evaluated at 0.98 eV ( $\sim$ 1250 nm) by fitting the absorption data to the equation $\sigma \cdot \hbar\omega = A(\hbar\omega - E_g)$ [17], where $\sigma$ is the absorption coefficient, $\hbar\omega$ is the photon energy and $E_g$ is the direct band gap, following a method suggested by Wang et al. [16] (Fig. 6). Using the theoretical model developed by Wang to correlate the blue shift to the particle size, this absorption edge corresponds to a particle size of about 5 nm, in good agreement with XRD results. Non-linear measurements were performed on several PbS doped samples at 1.064 $\mu$m by the m-line technique using a pulsed (8 ns) Nd:YAG laser light source. Figure 7 shows five m-lines recorded at five different (increasing) incident light intensities. The results of four successive low and high intensity measurement cycles are reported in the same Fig. 7, to demonstrate the reversibility of the non-linear effect at this time scale. For high intensity a shift of about 0.1° of the minimum towards smaller angles is observed. This phenomenon corresponds to a

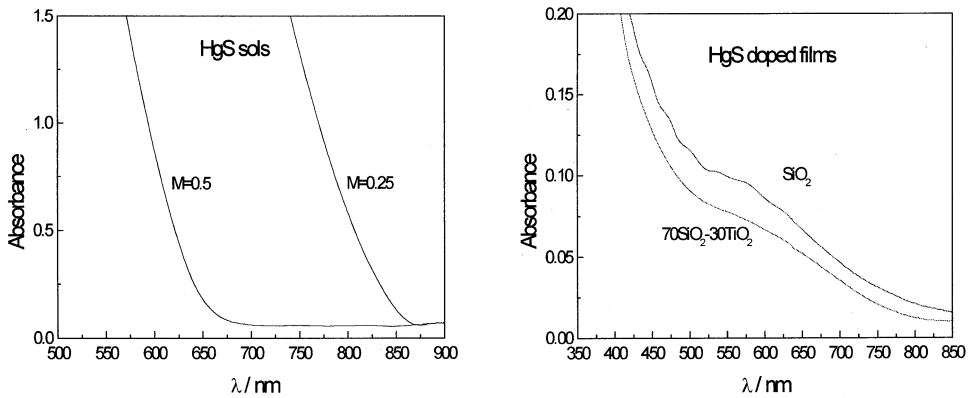


*Fig. 4.* Absorption curves of HgS colloidal sols prepared with $T = 1$ and different $M$ ratios (left) and HgS-doped films obtained from colloidal sols with $T = 1$ and $M = 0.5$.

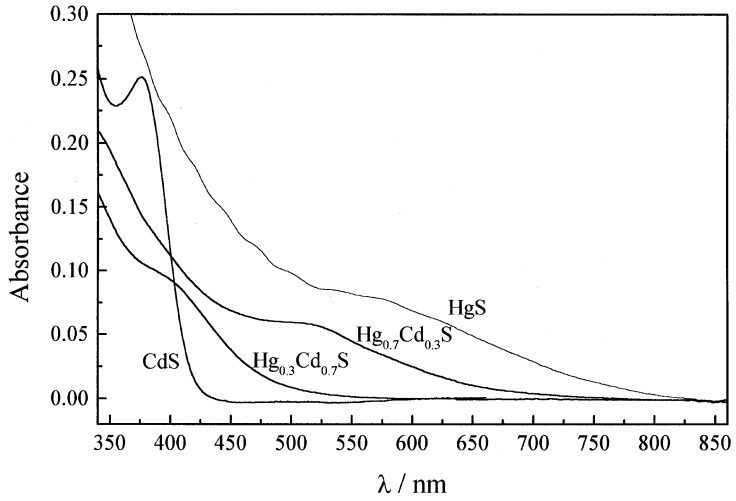


*Fig. 5.* Absorption curves of $Hg_xCd_{1-x}S$-doped silica films dried at 60°C. An *M* ratio of 0.5 was used.

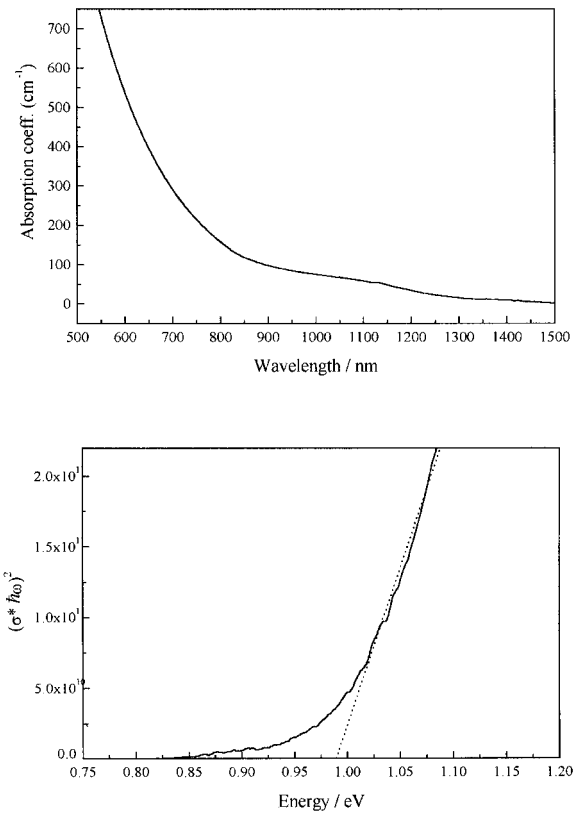


*Fig. 6.* Absorption spectra of PbS particles in $SiO_2$-$TiO_2$ film fired 1 h at 300°C in nitrogen (top). The spectra near the absorption edge are reported; the dotted line represents the theoretical direct band gap (bottom).

negative non-linearity. Values of the non-linear refractive index $n_2$, deduced from these measurements, ranged between $-5\ 10^{-9}$ and $-2\ 10^{-8}\,cm^2/kW$ depending on the sample [18].

Recently the non-linear refractive index of PbS-doped silica-titania waveguides was measured in the absorption region at 532 nm using two different techniques: non-linear m-lines and degenerate four-wave mixing. The value of the nonlinear refractive index measured by the m-line technique was $n_2 = -2\ 10^{-7}\,cm^2/kW$, much larger than the results reported above, obtained on similar samples in the transparent spectral region at 1.064 $\mu$m. The value obtained by the DFWM technique was, instead, $|n_2| = 5\ 10^{-9}\,cm^2/kW$. The difference between the values obtained by the two techniques was explained by the different durations of the laser pulses: 7 ns for m-lines and 30 ps for DFWM. This result shows that problems can arise when the optical non-linearities measured by different techniques are compared.

## 4. Optically Active Ions Doped Sol-Gel Films as IO Amplifiers

Studies of rare earth-doped sol-gel glasses, with particular emphasis on erbium, have recently been carried out [19,20] with the goal to develop amplifier materials for IO devices. The main problem related to sol-gel processing is the large amount of residual hydroxyl impurities, which act as quenching sites for

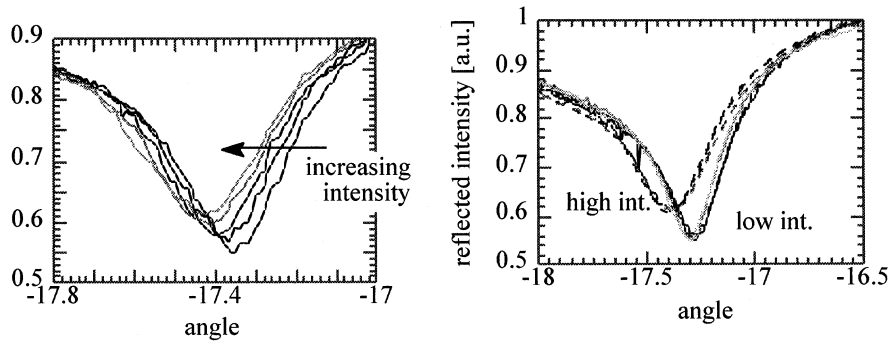


*Fig. 7.* Non-linear m-line measurement at 1064 nm for a PbS-doped silica-titania waveguide.

the active ions. Several methods to reduce the hydroxyl content have, therefore, been developed [21,22].

Our work has been focused on germania-based thin films doped with erbium. In a first step we have studied different $GeO_2$ based systems to select the most suitable matrix and in a second step we have optimized the selected system with respect to heat treatment, erbium precursor and co-dopant concentration.

### *4.1. Preparation and Characterization of Active Planar Waveguides Doped With $Er^{3+}$*

$Ge(OEt)_4$ (TEOG) and $Si(OEt)_4$ (TEOS) were used as precursors for germania and silica respectively. In the $P_2O_5$ co-doped samples, $P_2O_5$ powder dissolved in ethanol was used as a precursor. For $Al_2O_3$ co-doped samples, $Al(OBu)_3$ was mixed with the $GeO_2$-$SiO_2$ precursor solution. In the final solution $ErCl_3$ dissolved in ethanol and/or $Yb(NO_3)_3$ dissolved in methanol were added, with different molar ratios with respect to the total oxide concentration. A similar procedure was used for the compositions: $80GeO_2$-$20Nb_2O_5$, $80GeO_2$-$20SnO_2$, $80GeO_2$-$20TeO_2$ and $80GeO_2$-$20TiO_2$. In these systems TEOG dissolved in absolute ethanol was mixed with an ethanol solution of $Nb(OEt)_5$, $Sn(OBu)_4$, $Ti(OBu)_4$ or $Te(OEt)_4$. The dopants were added following the procedure used for the $GeO_2$-$SiO_2$ system. Details about the preparation of the solutions are described in [23].

Films were deposited on silica substrates by spinning and heating each layer at 600°C or 700°C for 15 min. Multilayer films with a thickness of up to 2 $\mu$m were obtained.

*Table 2.* Refractive index ($\lambda = 633$ nm) and fluorescence lifetimes of samples with different compositions fired at 600°C (nm = not measurable; na = no sample available)

| | | Co-dopants (10%) | | | | | |
|---|---|---|---|---|---|---|---|
| | | None | | $Al_2O_3$ | | $P_2O_5$ | |
| | $Er^{3+}$ [%] | n | $\tau$ [ms] | n | $\tau$ [ms] | n | $\tau$ [ms] |
| $GeO_2$ | 0.2 | 1.62 | nm | na | na | 1.61 | 1.6 |
| $80GeO_2$-$20TeO_2$ | 0.5 | 1.56 | nm | na | na | na | na |
| $80GeO_2$-$20SnO_2$ | 0.5 | 1.64 | nm | 1.67 | 1.8 | 1.63 | nm |
| | 1 | | 1.2 | | nm | | nm |
| $80GeO_2$-$20TiO_2$ | 0.1 | 1.65 | 2.7 | na | na | nm | nm |
| | 0.2 | | 2.7 | 1.68 | 2.3 | na | na |
| $80GeO_2$-$20Nb_2O_5$ | 0.5 | 1.76 | nm | 1.77 | nm | 1.77 | 2.7 |
| $80GeO_2$-$20SiO_2$ | 0.2 | 1.58 | 4 | 1.59 | nm | 1.58 | 4 |
| | 0.5 | | nm | | | | 3.5 |

The active properties of the planar waveguide samples were characterized by fluorescence spectra and lifetime measurements. In both cases the erbium ions were pumped by a laser diode emitting at 980 nm. Optical losses and refractive index of the thin film samples were also measured.

### *4.2. Host Matrices*

A critical problem in sample preparation was the tendency of $GeO_2$ gels to crystallize during thermal treatment. For this reason $80GeO_2$-$20M_xO_y$ ($M$ = Nb, Si, Sn, Ti, Te) films were heated at no more than 600°C (400°C for $80GeO_2$-$20TeO_2$). The fluorescence properties of these samples together with one pure $GeO_2$ reference sample were measured. The influence of $Al_2O_3$ and $P_2O_5$ on the active properties of the films was also studied.

Raman and infrared spectroscopy were performed to verify if the phonon energy of these systems is lower than that of the silica based systems. The investigations (see Fig. 8) showed that the highest absorption frequencies are revealed by IR spectroscopy: they are at $\approx 870\,cm^{-1}$ for all $GeO_2$ based systems. In silica containing matrices there is, of course, also a vibration at $1100\,cm^{-1}$, but this should not affect too much the overall phonon relaxation process in matrices were $GeO_2$ is predominant. Absorption at higher frequencies can be considered negligible because they are weak both in Raman and IR spectroscopy.

For some of the samples we found problems with the sol-gel process. In the case of the $TeO_2$ co-doped matrix we did not succeed in making films that were thick enough to support a guided mode at the fluorescence wavelength. The measurement of the fluorescence properties was, therefore, not possible on these samples. The $GeO_2$-$Nb_2O_5$ matrices, on the other hand, exhibited large linear waveguide losses, which we assume to be caused by structural problems of the matrix.

Figure 9 shows the fluorescence of three representative samples (all samples with 10% $Al_2O_3$ and 0.5% $Er^{3+}$) of this series ($M$ = Nb, Sn, Ti). The shapes of the spectra are similar with a peak at 1540 nm and a shoulder on the long wavelength side of the peak. The fluorescence lifetimes of the samples are given in Table 2. With the exception of the $TiO_2$ co-doped sample the positive influence of $P_2O_5$ or $Al_2O_3$ co-doping can be clearly seen. In general, the lifetimes are in the 1–2 ms range, too low for any real application. The best results were obtained for the $80GeO_2$-$20SiO_2$ system that has a lifetime up to 5 ms in the $P_2O_5$ co-doped case. This matrix was selected for further investigation and optimization even though we could not find any fluorescence in the $Al_2O_3$ co-doped sample of that composition.

### *4.3. OH-Treatments*

The short erbium lifetimes in the samples are probably due to the high concentration of OH-groups in samples fabricated by sol-gel processing. The high local phonon energy of these hydroxyl groups makes them act as efficient quenching centers for excited ions [24]. This is one of the most important drawbacks

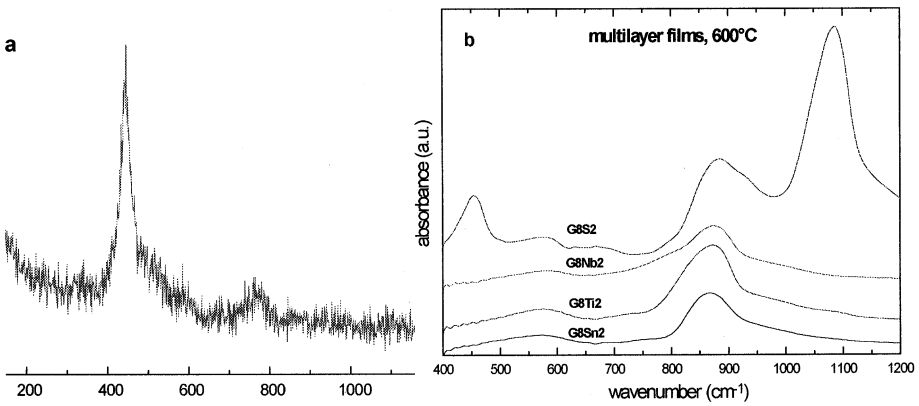


*Fig. 8.* Raman spectrum of (a) G8S2 powders and (b) FTIR spectra of multilayer films with 80% $GeO_2$.

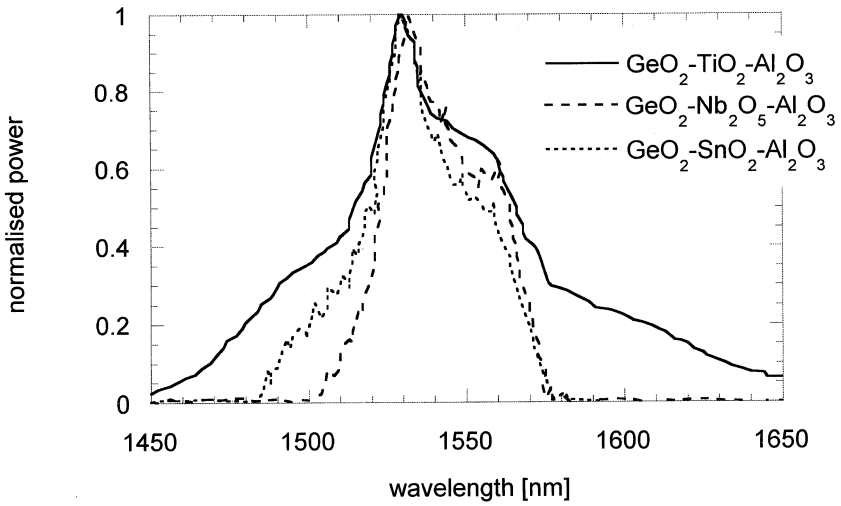


*Fig. 9.* Erbium fluorescence spectra of different host matrices.

of the sol-gel process. Furthermore, it was shown that this effect is even more important for samples containing a large amount of germania [25]. A commonly used technique to overcome this problem consists of a special heat treatment in carbon tetrachloride ($CCl_4$) [21]. We studied the effects of such a treatment at 500°C for a duration of 30 min. For the $P_2O_5$ doped samples this treatment increased the lifetime from 1 ms to 6.1 ms (0.2% $Er^{3+}$).

$Al_2O_3$ doped films have a much lower tendency to crystallize than the $P_2O_5$ doped ones. For this reason we can use higher temperatures without changing the morphology of the film. Samples, which had too weak to measure fluorescence, show lifetimes of up to 5.6 ms (0.2% $Er^{3+}$) after heat treatment at 700°C for 30 min. On some samples we did additionally the treatment used for the $P_2O_5$ doped samples (500°C in $CCl_4$), but we did not find any further improvement of the lifetimes.

The higher lifetimes measured in the $P_2O_5$ co-doped samples are attributed to a lower presence of OH groups, a characteristic seen in other sol-gel phosphate glasses [26]. These results show clearly the importance of reducing the OH concentration of the films to obtain good active properties. For this reason we treated our samples systematically with the procedures described above.

### *4.4. Fluorescence Spectra and Lifetime*

Figure 10 shows the erbium fluorescence spectra of $GeO_2$-$SiO_2$ samples doped with 10% $P_2O_5$ or $Al_2O_3$ and 0.5% $Er^{3+}$. For the $P_2O_5$ doped sample we observed a peak at 1535 nm with a full width at half maximum (FWHM) of 20 nm. Several small peaks protrude on both sides of the main peak. This shape is very similar to the case of a pure $GeO_2$-$SiO_2$ matrix. The addition of $Al_2O_3$, on the other hand, broadens the spectrum and a pronounced shoulder on the long wavelength side appears. The FWHM increases to values greater than 40 nm. A similar trend was observed in the $Al_2O_3$ doped $GeO_2$-$TiO_2$ system (Fig. 9). The broadening of the spectra suggests that a wider distribution of $Er^{3+}$ bonding sites is present and that $Al_2O_3$ efficiently disperses $Er^{3+}$ in the matrix. Another effect of doping is the shift of the

*Table 3.* Solubility of $C_{60}$ derivatives 1, 2 and 3 (Scheme 1) in THF and fullerene concentrations in sol-gel matrix

| $C_{60}$ derivative | Solubility (M) in THF | $C_{60}$-R : $SiO_2$ molar ratio |
|---|---|---|
| 1 | $1.0\ 10^{-5}$ | $5.0\ 10^{-4}$ |
| 2 | $2.9\ 10^{-2}$ | $2.4\ 10^{-3}$ |
| 3 | $1.1\ 10^{-3}$ | $8.5\ 10^{-4}$ |

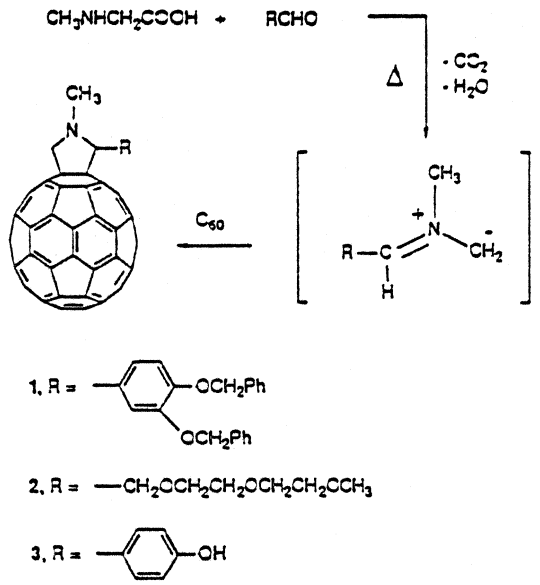


*Scheme 1.*

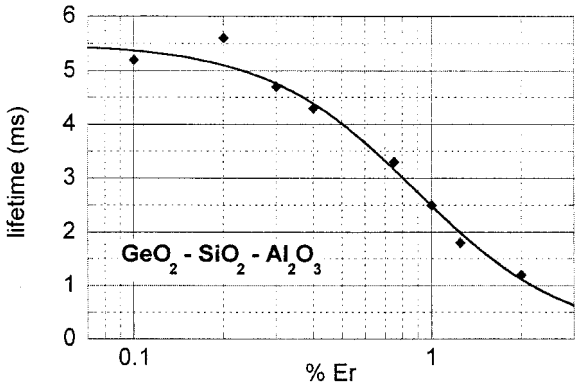


*Fig. 11.* Quenching curve of the $80GeO_2$-$20SiO_2$ matrix co-doped with 10% $Al_2O_3$. The deduced values for the maximum fluorescence lifetime and the quenching concentration are $\tau_0 = 5.5$ ms and $c_q = 0.9\%$, $p = 1.7$.

fluorescence maximum towards smaller wavelengths. This shift indicates an influence on the $Er^{3+}$ bonding environment. It seems that the Er-O bonding is more ionic in the presence of $Al^{3+}$ [19].

The $P_2O_5$ co-doped samples showed a strong tendency to become hygroscopic for larger concentrations of phosphorous. For this reason we limited the study of the influence of the co-dopants only to $Al_2O_3$. We investigated $GeO_2$-$SiO_2$ matrices co-doped with 5, 7.5, 10, and 12.5% of $Al_2O_3$ and doped with 0.5% $Er^{3+}$. For larger concentrations we found problems obtaining a homogeneous matrix. We did not observe any dependence of the shape of the fluorescence spectra on $Al_2O_3$ concentration. The spectral resolution of our spectrum analyzer was not sufficient to resolve the expected shift of the fluorescence maximum as a function of the $Al_2O_3$ concentration. The influence on the lifetime, however, was clearly measurable. In Fig. 12 the lifetime is recorded as a function of the $Al_2O_3$ concentration. We observed a sharp rise between 7.5% and 10%. The variations in lifetime are negligible both at smaller and larger concentrations. Because we obtained similar results for different sample series, we can exclude experimental errors. Our results indicate the existence of a threshold $Al_2O_3$ concentration necessary for efficient enhancement of the $Er^{3+}$ solubility in the matrix. This effect saturates for concentrations larger than 10%. Similar results were obtained by Arai on neodymium-doped silica glass [27].

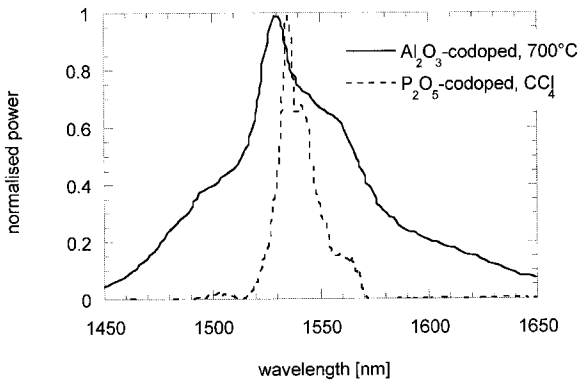


*Fig. 10.* Erbium fluorescence spectra of the $GeO_2$-$SiO_2$ matrices co-doped with $Al_2O_3$ or $P_2O_5$.

The quenching concentration in the $Al_2O_3$ doped system was determined by measuring samples with 0.1 to 2% $Er^{3+}$. For the sample series shown in Fig. 11 we used the two OH treatments described before (700°C and 500°C in $CCl_4$). The empirical equation:

$$\tau = \frac{\tau_0}{1 + (c/c_q)^p} \tag{1}$$

was used to deduce the quenching concentration $c_q$ and the maximum fluorescence lifetime in the zero-concentration limit $\tau_0$ ($p$ is a fitting parameter without physical meaning). The obtained values are

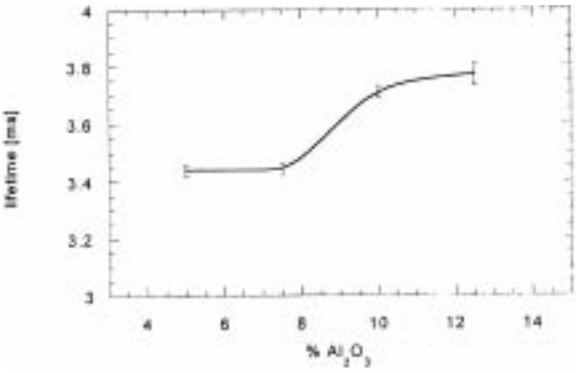


*Fig. 12.* Dependence of the erbium fluorescence (0.5% $Er^{3+}$) lifetime on $Al_2O_3$ concentration in the $GeO_2$-$SiO_2$-$Al_2O_3$ matrix. The line is a guide for the eye.

$\tau_0 = 5.5\,\text{ms}$ and $c_q = 0.9\%\ Er^{3+} (p = 1.7)$. The investigation of a second series using only the heat treatment at 700°C leads to similar values ($\tau_0 = 5.0\,\text{ms}$ and $c_q = 1\%\ Er^{3+}$). The values of $\tau_0$ are small compared to those obtained for $Er^{3+}$ doped germano-silicate materials prepared by other methods ($\sim 9\,\text{ms}$) [28]. But they are greater than published values for germano-silicate waveguides made by sol-gel ($\sim 3.5\,\text{ms}$ for 0.25% $Er^{3+}$) [25]. We think that this difference is due to the OH groups. Further improvements of the lifetime may be reached by suppressing the hydroxyl groups.

### *4.5. Additional Investigations*

Waveguide losses of about 2–3 dB/cm at 633 nm and 1.5 dB/cm at 840 nm were measured on $GeO_2$-$SiO_2$ multilayer films. Similar results were obtained by different authors [25,29]. Germano-silicate glasses are highly transparent in the visible and near infrared spectral region. The measured losses are, therefore, assumed to be mainly due to scattering arising from dust or other imperfections. The slightly smaller losses measured at longer wavelengths confirm this interpretation. Co-doping an erbium doped matrix with ytterbium enhances the absorption of the pump and thus the inversion of the laser level. We have tested Yb co-doping in $GeO_2$-$SiO_2$-$Al_2O_3$ and $GeO_2$-$SiO_2$-$P_2O_5$ matrices doped with 0.5% $Er^{3+}$ and the same amount of Yb. The fluorescence intensity increased by more than one order of magnitude, while the emission cross-section remained unchanged. As expected, the lifetimes of these samples were the same as the ones of the equivalent undoped Yb samples.

## 5. Fullerene Doped Sol-Gel Materials for Optical Limiting

$C_{60}$ [30,31] has been recently studied for its wide range of potential applications in materials science. In particular, $C_{60}$ exhibits optical limiting (OL) properties [32–35] a non-linear response to a laser fluence determined by a reverse saturable absorption (RSA). The incorporation of $C_{60}$ in a suitable matrix, leads to materials for optical limiting. These are passive devices, which exhibit a high linear transmission at low energy level and strongly and quickly reduce their transmittance with increasing laser fluence to a level that would not damage optical sensors or the human eye. The fluence is the relevant physical quantity that an optical limiting material should control, for eye protection against laser pulses in the nanosecond range or shorter.

We used functionalization of $C_{60}$ to increase the solubility in the sol-gel solution and to chemically link $C_{60}$ to the matrix network. $C_{60}$ is a reactive molecule and can be functionalized in several ways. The photophysics of fullerene derivatives has still to be fully explored, but the saturation of a double bond in $C_{60}$ does not seem to affect significantly the photophysical properties of the derivatives with respect to $C_{60}$ [36]. Actually, fullerene derivatives

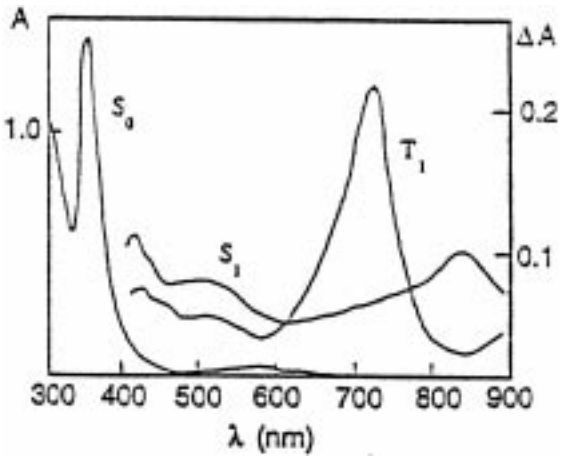


*Fig. 13.* Ground ($S_0$) state absorption, first excited singlet ($S_1$) and triplet ($T_1$) state difference absorption spectra of $C_{60}$ in toluene.

have a wider absorption range than $C_{60}$ [36]. Moreover, $C_{60}$ derivatives are usually more easily handled than $C_{60}$ itself and their solubility in organic solvents can be modulated. In particular, $C_{60}$ derivatives are usually more soluble than $C_{60}$ [37] in most organic solvents, while they retain the main electronic features [38–40]. The recently reported functionalization methodology, based in 1,3-dipolar cycloadditions of azomethine ylides to $C_{60}$, allows the preparation of a wide variety of substituted fulleropyrrolidines: compounds in which the 3,4-bond of a pyrrolidine ring is fused with a 6,6 ring junction of $C_{60}$ [41]. Fulleropyrrolidines functionalized at position 2 of the pyrrolidine ring and with different solubilities in tetrahydrofuran (THF) were synthesized.

Transparent films with $C_{60}/SiO_2$ molar ratio of $1.4\ 10^{-4}$ were obtained [42,43]. This corresponds to the first incorporation of $C_{60}$ in thin silica films, the $C_{60}$ concentration in the film (350 nm thick), however, was too low to observe clear signatures in the UV-vis spectra of the electronic transitions with high oscillator strength from the ground state to the 31T1u and to the 61T1u excited states, observed at 328.4 nm and 256.6 nm respectively in *n*-hexane solution [44].

The importance of solubility and chemical affinity is shown from the results obtained using fulleropyrrolidine with different functional groups in the position 2, whose synthesis is described elsewhere (Table 3). The compounds, moreover, are soluble in THF, a more appropriate solvent for both silicon alkoxides and water. Solubility data and fullerene concentrations in sol-gel samples are reported in Table 3.

Transparent, brownish films, 800 nm thick, were obtained with derivatives 1 and 3, while solutions of compound 2, which has the highest solubility, were not useful in film preparation due to the formation of microscopic clusters as shown by SEM on the thin films. However, compound 3 can be embedded at higher concentrations in sol-gel films than derivative 1 that is soluble as 3 in THF (Table 3). The higher affinity of 3 with the sol-gel matrix is responsible for the observed concentration effect. UV-vis spectra of the films containing compounds 1 and 3 are reported in Fig. 14. The two bands typical of the characteristic electronic transitions of $C_{60}$ can be observed also in the samples doped with 1 and 3, at about 260 and 330 nm.

The results of OL measurements on the silica matrix (monolithic samples of thickness of about 0.2 cm) and the same matrix doped with $C_{60}$ ($C_{60}$ : $SiO_2 = 5.4\ 10^{-5}$) and 3 ($1b : SiO_2 = 1.0\ 10^{-4}$) respectively, are reported in Fig. 15.

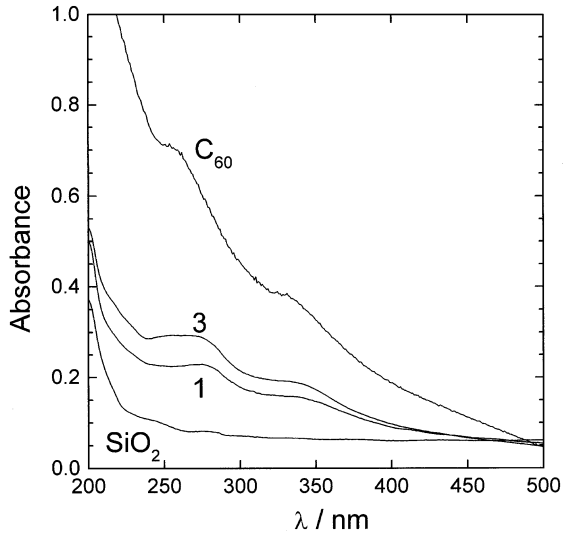


*Fig. 14.* UV-vis spectra of: (1) silica film; (2) silica film containing 1; (3) silica film containing 3; (4) powdered film containing $C_{60}$ dispersed in KBr.

The deviation of the absorption from linearity shows the OL effect due to fullerene, and is related not only to the intrinsic electronic properties of $C_{60}$, but also to its concentration in the matrix. Thus, the lower

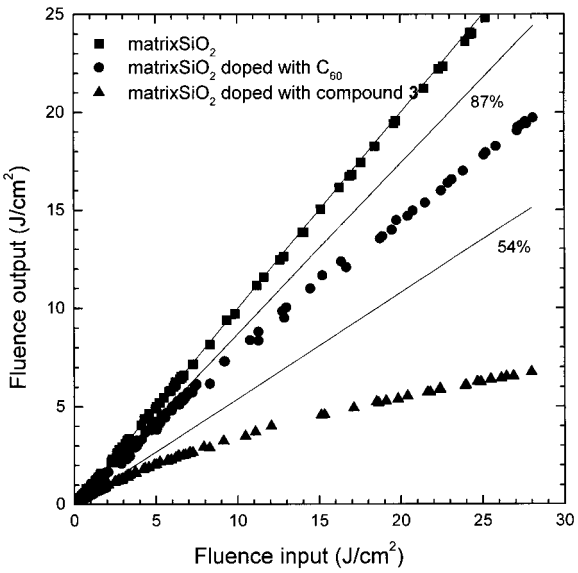


*Fig. 15.* OL data of silica monolith (squares), $C_{60}$ (circles) and 3 (triangles) in silica monoliths. Straight lines indicate the linear transmittance at low fluences for the different samples.

effect observed for unsubstituted $C_{60}$ with respect to 3 is due to its lower concentration and to its lower OL efficiency at the measurement wavelength. Noteworthy is the high transmittance of the matrix alone ( $\approx$ 100%), which indicates the very good optical quality of the material. From the comparison between OL data of $C_{60}$ and 3 in toluene solution and in the sol-gel matrix, it can be argued that the lower linear transmittance at low fluences in doped samples (straight lines in Fig. 15), is due to the absorption properties of the fullerenes and only partially to scattering losses.

Transmittance in doped gels is 87% for $C_{60}$ and 57% for compound 3. The latter is much better than the values of our previous results. The threshold for NL transmittance is similar to that reported for PMMA containing $C_{60}$ and the threshold for laser damage is very high. Both transmittance and damage threshold are important properties for the development of optical limiting devices.

More recent results show that an improvement of these sol-gel materials is obtained by using silicon-alkoxide functionalized fullerenes (Scheme 2). Their use, in fact, increases the concentration attainable and avoids the contribution of clustering to the linear scattering. Typical results of non-linear transmission measurements are shown in Fig. 16 and a summary of OL data measured for monolithic slabs containing different $C_{60}$-derivatives at three laser wavelengths is provided in Table 4.

OL behavior is always observed since $A_{20}/A_0$ (the relative absorbance at 20 J cm$^{-2}$) is greater than one in all cases. However, compared with results obtained for solution samples, the OL efficiency appears to be greatly reduced in the sol-gel materials. The likely origin of this is the linear scattering from the monolithic slabs. In fact, in most cases the linear transmission estimated by a linear fit of the low-fluence data is considerably lower than what is expected on the basis of the fullerene concentration and thickness of the slabs. Among the sol-gel samples measured, there is a general tendency of those containing an alkoxide functionality to give better results, especially for compound 1 e.

In conclusion, the results obtained indicate that with slabs of thickness in the millimeter range the linking of the fullerene derivatives to the silica matrix is, in general, not sufficient to warrant the required structural and optical homogeneity of the sol-gel material. On the other hand, the high solubility of our silicon-alkoxide-

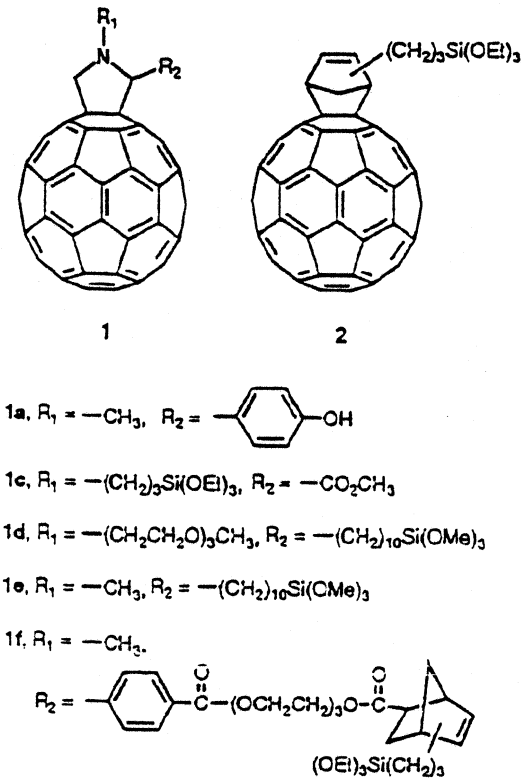


*Scheme 2.*

functionalized fullerenes allows, at least theoretically, to obtain a measurable OL effect in sol-gel films of some tens to a few hundreds $\mu$m thickness and to approach the realization of a bottleneck optical limiter based on a multilayer structure. In our very recent results, other types of organic-inorganic hybrid materials were considered and matrices of this type were prepared following procedures similar to those reported in literature. Films with a thickness up to 100 $\mu$m were deposited by spinning on glass substrates. These sols were suitable for embedding $C_{60}$-derivatives up to a concentration of 8.0 $10^{-3}$ moles per mole of silica precursor, without detecting any clustering phenomena by optical microscopy. These fullerene doped films, dried at 60°C, remained undamaged up to a fluence of 25 J cm$^{-2}$.

## 6. Conclusions

Sol-gel processing was used to fabricate several types of materials for integrated optics and photonics applications. Sol-gel processing was shown to be a very versatile technique to obtain inorganic and

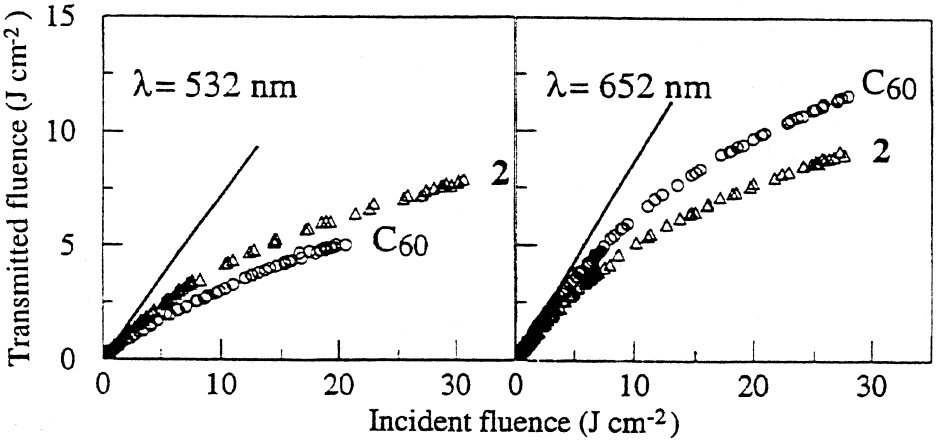


*Fig. 16.* Optical limiting data measured on toluene solution of $C_{60}$ and compound 2. For both solutions the linear transmittance was 72% at 532 nm (a) and 87% at 652 nm (b).

*Table 4.* Linear transmittance ($T_o$(%)) and relative absorbance at 20 J cm$^2$ ($A_{20}/A_o$) of $C_{60}$[a] and $C_{60}$ derivatives 1(a–f)—2 embedded in sol-gel coatings of thickness d (cm)

| | | 532 nm | | 581 nm | | 652 nm | |
|---|---|---|---|---|---|---|---|
| Sample | d (cm) | $T_o$(%) | $A_{20}/A_o$ | $T_o$(%) | $A_{20}/A_o$ | $T_o$(%) | $A_{20}/A_o$ |
| $C_{60}$[b] | 0.28 | 68 | 1.7 | 75 | 1.7 | 87 | 2.4 |
| 1a | 0.21 | 27 | 1.3 | 45 | 1.6 | 47 | 1.5 |
| 1a[c] | 0.23 | 38 | 1.5 | 50 | 2.1 | 55 | 2.2 |
| 1e | 0.25 | 30 | 2.0 | 50 | 2.3 | 79 | 5.4 |
| 1f | 0.20 | 45 | 1.9 | 55 | 2.2 | 53 | 2.5 |
| 2 | 0.15 | 70 | 2.3 | 80 | 3.0 | 65 | 1.6 |

[a]The $C_{60}/SiO_2$ molar ratio is 1.0 $10^{-4}$ M, unless otherwise specified.
[b]$C_{60}/SiO_2 = 5.4\ 10^{-5}$ M.
[c]1a/$SiO_2 = 5.0\ 10^{-5}$ M.

organic-inorganic materials. Furthermore, they have the advantage of simple deposition processes for coating films. These characteristics open many possibilities for wide development of photonic devices that are based on sol-gel processing and that can be market competitive with existing technologies and materials.

## References


1. *Sol-Gel and polymer Photonic Devices*, *SPIE Crit. Rev. Proc.*, **CR68**, Ed. M.P. Andrews and S.I. Najafi.
2. M. Guglielmi, P. Colombo, L.M.D. Esposti, G.C. Righini, and S. Pelli, *Glasses for Optoelectronics II*, *Proc. SPIE*, **1513**, 2 (1991).
3. M. Guglielmi, P. Colombo, L.M.D. Esposti, G.C. Righini, S. Pelli, and V. Rigato, *J. Non-Cryst. Solids*, **147 & 148**, 641 (1992).
4. S. Pelli, G.C. Righini, A. Verciani, M. Guglielmi, A. Martucci, and A. Scaglione, *Proc. SPIE*, **2213**, 58 (1994).
5. G. Brusatin, M. Guglielmi, P. Innocenzi, A. Martucci, G. Battaglin, S. Pelli, and G.C. Righini, *J. Non-Cryst. Solids*, **220**, 202 (1997).
6. P. Innocenzi, A. Martucci, M. Guglielmi, L. Armelao, S. Pelli, G.C. Righini, and G.C. Battaglin, *J. Non-Cryst. Solids*, **259**, 182 (1999).
7. P.G. Kik and A. Polman, *MRS Bulletin*, **23**(4), 48 (1998).
8. M. Guglielmi, *SPIE Crit. Rev. Proc.*, **CR68**, 186 (1997).
9. N. Tohge, M. Asuka, and T. Minami, *J. Non-Cryst. Solids*, **147 & 148**, 631 (1992).
10. A. Martucci, M. Guglielmi, and K. Urabe, *J. Sol-Gel Sci. Techn.*, **11**, 105 (1998).
11. E.H. Swift and E.A. Butler, *Anal. Chem.*, **28**, 146 (1956).
12. M. Guglielmi, A. Martucci, E. Menegazzo, G.C. Righini, S. Pelli, J. Fick, and G. Vitrant, *J. Sol-Gel Sci. Techn.*, **8**, 1017 (1997).
13. M. Guglielmi, A. Martucci, J. Fick, and G. Vitrant, *J. Sol-Gel Sci. Techn.*, **11**, 229 (1998).
14. L. Banyai, Y.Z. Hu, M. Lindberg, and S.W. Koch, *Phys. Rev. B*, **38**, 8142 (1988).

15. N.F. Borelli and D.W. Smith, *J. Non-Cryst. Solids*, **180**, 25 (1994).
16. Y. Wang, A. Suna, W. Mahler, and R. Kasowski, *J. Chem. Phys.*, **87**, 7315 (1987).
17. N.F. Mott and E.A. Davis, *Processes in Non-Crystalline Materials*, 273, Claredon, Oxford (1979).
18. J. Fick, G. Vitrant, A. Martucci, M. Guglielmi, and G.C. Righini, *Nonlinear characterization in the near infrared of PbS doped sol-gel thin films*, to be published on the Proc. of the Conf. On Lasers and Electro Optics Europe (CLEO-E), Amburg, (1996).
19. B.T. Stone and K.L. Bray, *J. Non-Cryst. Solids*, **197**, 136 (1996).
20. X. Fan, M. Wan, and G. Xiang, *Materials Letters*, **27**, 177 (1996).
21. J. Phalippou, T. Woignier, and J. Zarzycki, in: *Ultrastructure Processing of Ceramics, Glasses and Composites*, ed. L.L. Hench and D.R. Ulrich (Wiley, New York, 1984) p. 70.
22. E.J.A. Pope and J.D. Mackenzie, *J. Am. Cer. Soc.*, **76**, 1325 (1993).
23. G. Brusatin, M. Guglielmi, and A. Martucci, *J. Am. Cer. Soc.*, **80**, (1997) 3139.
24. R.H. Cole and E. Tombari, *J. Non-Cryst. Solids*, **131–133**, 969 (1991).
25. M. Benatsou and M. Bouazaoui, *Optics. Comm.*, **137**, 143 (1997).
26. R.R.A. Syms, V.M. Schneider, W. Huang, and M.M. Ahmad, *Elect. Lett.*, **33**, 1216 (1997).
27. K. Arai, H. Namikawa, K. Kumata, T. Honda, Y. Ishii, and T. Handa, *J. Appl. Phys.*, **59**, 3430 (1986).
28. B.J. Ainslie, *J. Lightwave Tech.*, **9**, 220 (1991).
29. K.D. Simmons, G.I. Stegeman, B.G. Potter, and J.H. Simmons, *J. Non-Cryst. Solids*, **179**, 254 (1994).
30. H.W. Kroto, J.R. Heath, S.C. O'Brien, R.F. Curl, and R.E. Smalley, *Nature*, **318**, 162 (1985).
31. W. Krätschmer, L.D. Lamb, K. Fostiropoulos, and D.R. Huffman, *Nature*, **347**, 354 (1990).
32. L.W. Tutt and A. Kost, *Nature*, **356**, 225 (1992).
33. J.W. Arbogast, A.P. Darmanian, C.S. Foote, Y. Rubin, F.N. Diederich, M.M. Alvarez, S.J. Anz, and R.L. Whetten, *J. Phys. Chem.*, **95**, 11 (1991).
34. Y. Wang, *Nature*, **356**, 585 (1992).
35. F. Kajzar, C. Taliani, R. Danieli, S. Rossini, and R. Zamboni, *Chem. Phys. Lett.*, **217**, 418 (1994).
36. J.L. Anderson, Y.-Z. An, Y. Rubin, and C.S. Foote, *J. Am. Chem. Soc.*, **116**, 9763 (1994).
37. R.S. Ruoff, D.S. Tse, R. Malhotra, and D.C. Lorents, *J. Phys. Chem.* **97**, 3379 (1993).
38. F. Wudl, *Acc. Chem. Res.* **25**, 157 (1992).
39. R. Taylor and D.R.M. Walton, *Nature*, **363**, 685 (1993).
40. A. Hirsch, *Angew. Chem. Int. Ed. Engl.*, **32**, 1138 (1993).
41. M. Maggini, G. Scorrano, and M. Prato, *J. Am. Chem. Soc.*, **115**, 9798 (1993).
42. M. Maggini, G. Scorrano, M. Prato, G. Brusatin, P. Innocenzi, M. Guglielmi, A. Renier, R. Signorini, M. Meneghetti, and R. Bozio, *Adv. Mater.*, **7**, 404 (1995).
43. M. Prato, M. Maggini, G. Scorrano, G. Brusatin, P. Innocenzi, M. Guglielmi, M. Meneghetti, and R. Bozio, *Mat. Res. Soc. Symp. Proc.*, **359**, 351 (1995).
44. M. Maggini, G. Scorrano, M. Prato, G. Brusatin, M. Guglielmi, M. Meneghetti, and R. Bozio, *Fullerenes: Recent Advances in the Chemistry and Physics of Fullerenes and Related Materials*, edited by R.S. Ruoff and K.M. Kadish (The Electrochem. Soc. Inc., Pennington N.J.), **95–10**, 84–89 (1995).